Asymmetric Fermi superfluid in a harmonic trap

2006 J. Phys.: Condens. Matter 18 5567

(http://iopscience.iop.org/0953-8984/18/23/025)

INSTITUTE OF PHYSICS PUBLISHING JOURNAL OF PHYSICS: CONDENSED MATTER

J. Phys.: Condens. Matter **18** (2006) 5567–5577 doi:10.1088/0953-8984/18/23/025

Asymmetric Fermi superfluid in a harmonic trap

C-H Pao[1] **and S-K Yip**[2]

[1] Department of Physics, National Chung Cheng University, Chiayi 621, Taiwan
[2] Institute of Physics, Academia Sinica, Nankang, Taipei 115, Taiwan

E-mail: pao@phy.ccu.edu.tw

Received 27 March 2006
Published 26 May 2006
Online at stacks.iop.org/JPhysCM/18/5567

Abstract

We consider a dilute two-component atomic fermion gas with unequal populations in a harmonic trap potential using the mean field theory and the local density approximation. We show that the system is phase separated into concentric shells with the superfluid in the core surrounded by the normal fermion gas both on the weak-coupling BCS side and near the Feshbach resonance. On the strong-coupling BEC side, the composite bosons and left-over fermions can be mixed. We calculate the cloud radii and compare axial density profiles systemically for the BCS, near resonance and BEC regimes.

(Some figures in this article are in colour only in the electronic version)

1. Introduction

The original BCS state for superconductors considers pairing between two species of fermions with equal populations. For a long time, theorists studied the fermion system with unequal species, or mismatched Fermi surfaces, and proposed this system may have a different ground state [1], in particular the so called Fulde–Ferrell–Larkin–Ovchinnikov (FFLO) phase. Experimentally, however, such superfluid states remain unclear because of the difficulty in preparing the magnetized superconductors.

Experiments with ultra-cold atoms have opened a new era to study this fermion system with unequal populations. Through the Feshbach resonance [2], the effective interaction between atoms can be varied over a wide range such that the ground state can be turned from a weak-coupling BCS superfluid to a strong-coupling Bose–Einstein condensation (BEC) regime. In the homogeneous system, theoretical studies [3–5] of the unequal fermion species show that the phase transition must occur when the resonance is crossed, in contrast to the equal population case where a smooth crossover takes place [6, 7]. Breached pair phase [8], phase separated states are also proposed [9, 10] in this system.

Two recent experiments [11, 12] studied the trapped ^{6}Li atoms with imbalanced spin populations and obtained the density profiles for various population differences. Both groups

found the system contains a superfluid core surrounded by normal fermions and provide evidence for phase separation near the crossover.

In this paper, we study this imbalanced fermion system by the mean field approximation and evaluate the density profiles for various coupling strengths from weak-coupling BCS superfluid to strong-coupling BEC regime. In particular, we calculate the axial density profiles, superfluid and minority cloud radii, and distinguish between the phase separation and Bose–Fermi mixture regimes. This paper is organized as follows. In section 2 we briefly review the mean-field approximation for the dilute fermion atoms with unequal populations. In section 3 we present our results for various polarizations from weak-coupling BCS superfluid to strong-coupling BEC side. We show that the axial density profiles are constant within the superfluid core and decrease beyond the phase boundary for the phase separations but are smoothly decreasing functions for the entire trap for the mixtures. Finally, we conclude with a briefly summary in section 4.

While this work was in progress, several theoretical papers have also studied the same problem under similar approximations [13–16] or going beyond [17, 18]. Basically, [13–17] also conclude the system is phase separated into concentric shells with superfluid in the centre and surrounding by leftover fermions near the resonance. The strong-coupling BEC limit has also been studied [13, 14, 18]. In this case, the composite bosons and unpaired fermions can mix. As the population difference increases the unpaired fermions can even penetrate into the superfluid core. Our paper provides a more systematic study of the entire BCS–BEC regimes for all polarizations.

2. Formalism

Restricting ourselves to wide Feshbach resonance, the two-component fermion system can be described by an effective one-channel Hamiltonian

$$H = \sum_{\mathbf{k},\sigma} \xi_\sigma(\mathbf{k}) c^\dagger_{\mathbf{k},\sigma} c_{\mathbf{k},\sigma} + g \sum_{\mathbf{k},\mathbf{k}',\mathbf{q}} c^\dagger_{\mathbf{k}+\mathbf{q},\uparrow} c^\dagger_{\mathbf{k}'-\mathbf{q},\downarrow} c_{\mathbf{k}',\downarrow} c_{\mathbf{k},\uparrow}, \tag{1}$$

where $\xi_\sigma(\mathbf{k}) = \hbar^2 k^2/2m - \mu_\sigma$ and the index σ runs over the two spin components. Within the BCS mean field approximation at zero temperature, the excitation spectrum in a homogeneous system for each spin is (see e.g. [20] for details)

$$E_\sigma(\mathbf{k}) = \frac{\xi_\sigma(\mathbf{k}) - \xi_{-\sigma}(\mathbf{k})}{2} + \sqrt{\left(\frac{\xi_\sigma(\mathbf{k}) + \xi_{-\sigma}(\mathbf{k})}{2}\right)^2 + \Delta^2}, \tag{2}$$

where $\xi_\sigma(\mathbf{k}) = \hbar^2 k^2/2m - \mu_\sigma$ are the quasi-particle excitation energies for normal fermions, and $-\uparrow \equiv \downarrow$. For an inhomogeneous system, e.g. the system in a harmonic trap, a finite system sized effect should be included [19]. However, the system can be treated as homogeneous locally if the number of particles is sufficiently large. A local density approximation, or Thomas–Fermi approximation (TFA), is applied and the chemical potential for spin σ is replaced by

$$\mu_\sigma(r) = \mu^0_\sigma - \tfrac{1}{2} m\omega^2 r^2, \tag{3}$$

with ω the isotropic trap frequency and r the distance from the trap centre. We shall show results explicitly only for the isotropic trap. In the local density approximation, the densities $n_\sigma(\mathbf{r})$ depends only on the local chemical potentials $\mu_\sigma(\mathbf{r})$. Hence the density profile of an anisotropic trap can be related to an isotropic one by rescaling the spatial coordinates appropriately. We then introduce the average chemical potential

$$\mu(r) \equiv \tfrac{1}{2}[\mu_\uparrow(r) + \mu_\downarrow(r)] = \mu_0 - \tfrac{1}{2} m\omega^2 r^2, \tag{4}$$

and the difference $h \equiv [\mu_\uparrow(r) - \mu_\downarrow(r)]/2 = (\mu_\uparrow^0 - \mu_\downarrow^0)/2$. The dispersion relation in equation (2) becomes

$$E_{\uparrow,\downarrow}(\mathbf{k}, \mathbf{r}) = \sqrt{\xi(\mathbf{k}, \mathbf{r})^2 + \Delta^2(\mathbf{r})} \mp h \tag{5}$$

where $\xi(\mathbf{k}, \mathbf{r}) \equiv \hbar^2 k^2/2m - \mu(r)$. We take spin up to be the majority species so that h and $E_\uparrow$ are positive always. Then the density profiles in a harmonic trap are

$$n_s(r) = n_\uparrow(r) + n_\downarrow(r) = \int \frac{\mathrm{d}^3k}{(2\pi)^3}\left[1 - \frac{2\xi(\mathbf{k}, \mathbf{r})}{E_\uparrow + E_\downarrow} f(-E_\uparrow)\right], \tag{6}$$

$$n_d(r) = n_\uparrow(r) - n_\downarrow(r) = \int \frac{\mathrm{d}^3k}{(2\pi)^3} f(E_\uparrow), \tag{7}$$

and the total number of particles $N = \int \mathrm{d}^3r n_s(r)$. Here f is the Fermi function. The polarization of the system is defined as

$$P \equiv \frac{N_\uparrow - N_\downarrow}{N} = \frac{1}{N}\int \mathrm{d}^3r n_d(r). \tag{8}$$

Now the pairing field Δ depends on position also. In the local density approximation, it obeys an equation similar to the homogeneous case [4, 20]:

$$-\frac{m}{4\pi a}\Delta(r) = \Delta(r)\int \frac{\mathrm{d}^3k}{(2\pi)^3}\left[\frac{1 - f(E_\uparrow) - f(E_\downarrow)}{E_\uparrow + E_\downarrow} - \frac{m}{\hbar^2k^2}\right]. \tag{9}$$

For a given scattering length a, we solve equations (6), (7) and (9) self-consistently for fixed total number of particles N and polarization P. The solutions to the 'gap equation' (9) may not be unique. The physical solution is determined by the condition of minimum free energy among the multiple solutions. We describe the detailed procedures in appendix A.

3. Results and discussions

In this section, we investigate the density profiles for various polarizations and coupling strengths from positive detuning BCS superfluid to negative detuning BEC side. With the aid of density profiles, we evaluate the radii of the superfluid phase boundaries for various cases and compare to the current experimental results. We close this section with a discussion of axial density profiles. Phase separation versus Bose–Fermi mixture can be clarified through the axial density profiles of the population difference.

In figure 1, we plot the radial density profiles for three different coupling strengths $1/k_Fa = -0.61, 0.03$, and 2.44 (for different columns) with polarization $P = 0.2, 0.5$, and 0.9 (for different rows). The total number of particles is fixed to 2×10^5. Here k_F is the Fermi wavevector at the trap centre for an ideal symmetric Fermi gas with the same total number of particles. In all these plots, the system shows a superfluid cloud surrounded by a normal Fermi gas except the case in figure 1(c) where the system is completely in the normal state with the polarization $P = 0.9$. It is consistent with the experimental observation [11] that the superfluid is destroyed by a sufficiently large population difference. We remark here however that the critical population difference P_c for the destruction of superfluidity obtained here is much larger than that found in the experiment [11]. For $1/k_Fa = -0.61$ here, $P_c > 0.6$ theoretically whereas an extrapolation of the data of [11] gives $P_c < 0.3$ (see further discussions below). For a less polarized system on the BCS side (figures 1(a) and (b)), it shows a clear phase separation between the superfluid and a normal Fermi gas. Note that within the superfluid cloud the population difference is zero and the system is just like the typically unpolarized superfluid. Outside the superfluid cloud both components of the fermions exist in the normal state, which

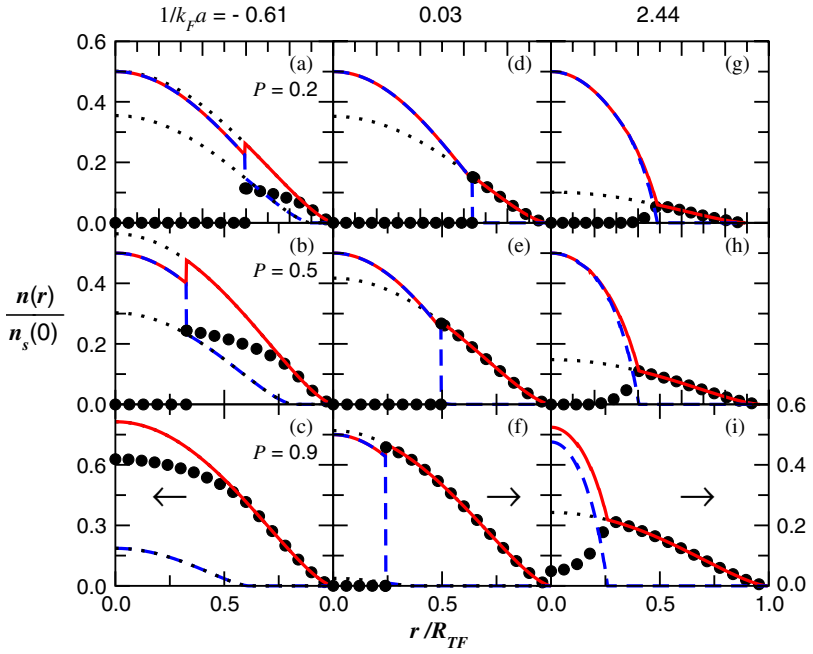

Figure 1. Radial density profiles for $n_\uparrow(r)$ (solid lines), $n_\downarrow(r)$ (dashed lines), and $n_\mathrm{d}(r)$ (solid circles). The dotted lines are the normal state density profile with the same density as in the normal region. The coupling strengths (each column) $1/(k_\mathrm{F}a) = -0.61$ (left, BCS side), 0.03 (middle, near resonance), 2.44 (right, BEC side) and the polarizations (each row) $P = 0.2$, 0.5, and 0.9. The total number of fermions is fixed to $N = 2.0 \times 10^5$. R_TF is the size of the Thomas–Fermi radius of the normal spin-up cloud.

indicates a fraction of the fermions which are not paired up even at the zero temperature. The density profile of the population difference $n_\mathrm{d}(r)$ peaks at the superfluid phase boundary and decreases gradually toward the edge of the trap. Its value is equal to the density profile of the majority when $r \geqslant r_\downarrow$, the radius of the minority cloud. At the superfluid phase boundary, both the majority and minority density profiles exhibit a discontinuous nature, which has also been observed by others [13–15].

Near resonance (figures 1(d)–(f)), similar phase separated states are observed. However, most of the minority are paired up in this regime such that the density profiles contain mainly the excess fermions outside the superfluid cloud at all Ps. This is consistent with the homogeneous normal phase boundary extending near resonance to large population difference [4]. Near resonance, the superfluid core survives at $P = 0.9$ in our calculations, whereas experimentally [11] it vanishes already at $P \approx 0.7$.

On the BEC side (figures 1(g)–(i)), all of the minority are paired up and the excess fermions can penetrate into the superfluid core. The system contains a superfluid core for any P (if sufficiently deep in the BEC regime; see figure 4 below). The system then contains three different phases: the purely superfluid, the mixture phase, and the normal fermions from the trap centre to the edge of the trap. The mixture phase extends toward the trap centre as the polarization increases. In figure 1(i) ($P = 0.9$), the system is highly polarized and the excess fermions extend deeply into the trap centre. In appendix B, we give an analytic discussion of the density profiles in the BEC limit.

The radius r_s of the superfluid core is one of the most interesting quantities in current studies of the imbalanced fermion system [12, 14–17]. From figure 1, the density profiles of

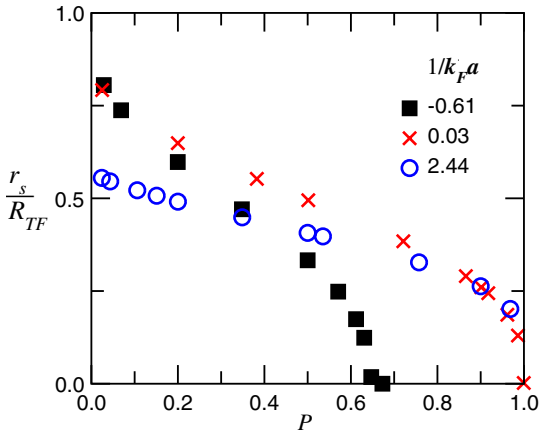

Figure 2. Radii of the superfluid core r_s versus polarization P for normalized coupling strengths in the legend.

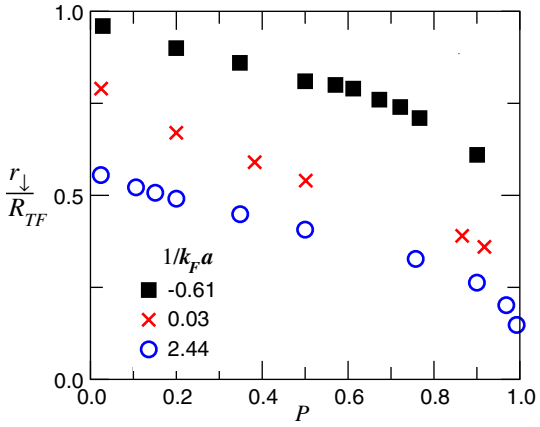

Figure 3. Radii of the minority species $r_\downarrow$ versus polarization P for normalized coupling strengths in the legend.

the population difference $n_d(r)$ have maxima at the phase boundaries between the superfluid and the normal fermions. r_s is thus also the peak position of $n_d(r)$. In figure 2, we plot r_s as a function of P for three different coupling strengths. r_s behaves quite differently above and below the resonance. On the BCS side the superfluid is eliminated when the polarization reaches around 0.65 for $1/(k_Fa) = -0.61$ and the system becomes completely normal with mismatch Fermi surfaces beyond this critical polarization. For large coupling strengths, r_s is finite except when P is exactly unity, since the superfluid is stable for any finite ($\neq 1$) polarization in the homogeneous case [4]. Except for small ($P \leqslant 0.1$) or large ($P \geqslant 0.9$) polarizations, the sizes of the superfluid clouds have maxima near the Feshbach resonance at fixed polarization.

We also plot the radii ($r_\downarrow$) of the minority (spin down fermions) cloud in figure 3. Below the Feshbach resonance, this radius is the same as the radius of the superfluid core because all the minority of fermions are paired up. However, this will not be true above the Feshbach resonance where part of the minority are not paired up in this regime. Unlike r_s, $r_\downarrow$ decreases

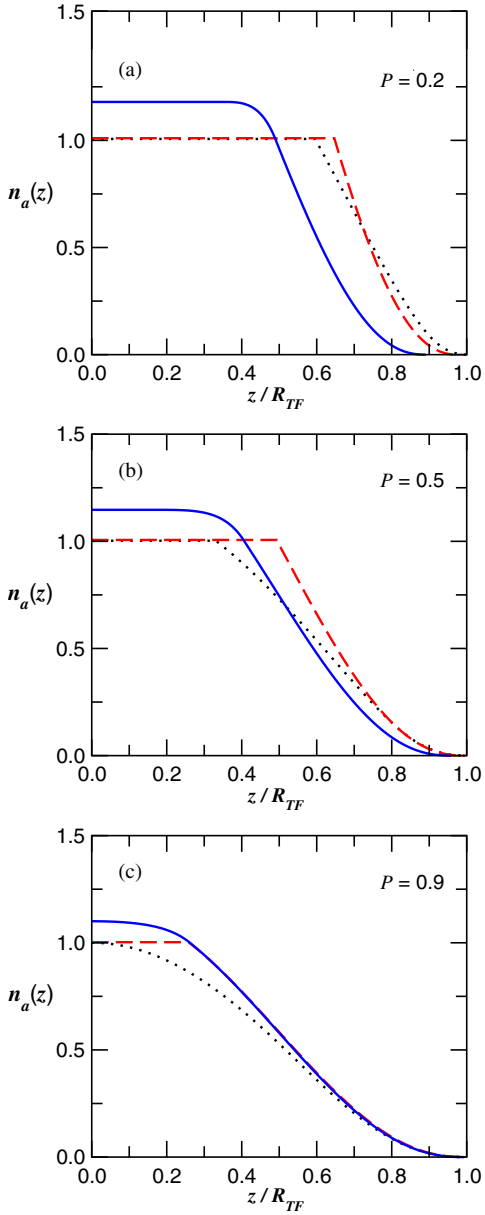

Figure 4. Axial population density difference $n_a(z)$ versus $z/R_{\rm TF}$. $R_{\rm TF}$ is defined in the caption of figure 1. $n_a(z)$ is normalized to 1 at $z = r_s$.

monotonically as the coupling strength increases. These two radii become identical when the minority are paired up completely when the system reaches the BEC regime.

Due to the experimental constraints, one cannot measure the radial density profiles directly. Instead, the axial density profiles are reported in [12]. In figure 4, we plot the normalized axial density profiles $n_a(z)$ [$\equiv \int {\rm d}x{\rm d}y n_{\rm d}(\vec{r})$] of the population difference for different coupling strengths at three fixed polarization P. For the cases with phase separations (figures 1(a), (b),

and (d)–(f)), the corresponding $n_a(z)$ are constants for $z \leqslant r_s$ and have a kink at the phase boundary (for $z = r_s$). This feature results from the population difference $n_d(r)$ being zero inside the superfluid cloud (see appendix C in detail) such that $n_a(z)$ remains the same value as at the phase boundary $z = r_s$. For a system with a mixed phase region (figures 1(g)–(i)), $n_a(z)$ increases smoothly toward the trap centre even as $z \leqslant r_s$. It reaches a constant value within the cloud containing superfluid only (e.g. the cases with solid lines in figures 4(a) and (b)). At large polarization (solid line in figure 4(c)), the excess fermions mix with superfluid entirely for $1/k_F a = 2.44$ such that $n_a(z)$ increases monotonically toward the trap centre. The completely different features for the axial density profiles of the population difference inside the superfluid cloud can help us to clarify whether the system is phase separation or mixture.

4. Conclusion

We have investigated the radial density profiles of the two-component fermion system with unequal spin populations under Feshbach resonance. The system shows a superfluid cloud in the trap centre surrounded by normal fermions. On the weak-coupling BCS side, the superfluid is destroyed completely at the polarization $P \gtrsim 0.65$ for $1/(k_F a) = -0.61$. Near the Feshbach resonance, almost all the minority are paired up and the system is phase separated into superfluid and the normal fermions. On the strong-coupling BEC side, the excess fermions can mix with the superfluid and the system contains three different phases, the purely superfluid cloud, the mixture phase, and the normal fermions from the trap centre to the edge of the trap.

In particular, we emphasize the difference in the axial density difference profiles between the phase separation and Bose–Fermi mixture regimes. The former shows a constant for $z < r_s$ and has a kink at the phase boundary but the latter are smoothly increasing toward the trap centre. However, reference [12] reported positive slopes of the axial density different profiles inside the superfluid cloud that indicates the $n_d(\vec{r})$ need to be negative somewhere within the superfluid cloud. We do not obtain this phenomenon within the current local density approach.

Acknowledgments

This research was supported by the National Science Council of Taiwan under grant numbers NSC94-2112-M-194-001 (CHP) and NSC94-2112-M-001-002 (SKY), with additional support from the National Center for Theoretical Sciences, Hsinchu, Taiwan.

Appendix A. Free energy

To determine the minimum free energy state when there are multiple solutions, we need an expression for the free energy. We obtain this as follows. First consider a system with fixed volume V and particle numbers N_σ. With the Hamiltonian in equation (1), it is straightforward to show that [21] the energy $E(N_\sigma, g)$ of this system obeys

$$\frac{\partial E}{\partial g} = \frac{V}{g^2}|\Delta|^2. \tag{A.1}$$

We need to eliminate g in favour of the scattering length a, the physical parameter of the system. These two variables are related by the expression

$$\frac{m}{4\pi\hbar^2 a} = \frac{1}{g} + \frac{1}{V}\sum_{\vec{k}} \frac{1}{2\epsilon_k}. \tag{A.2}$$

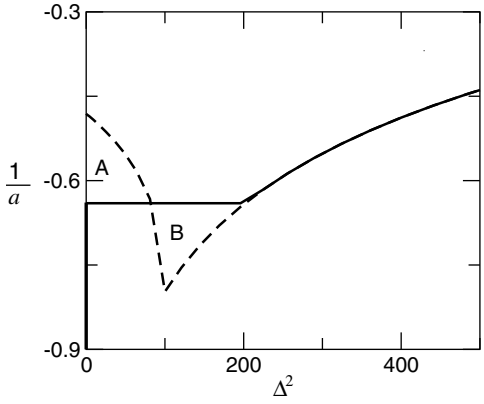

Figure A.1. Solution to the gap equation plotted as $1/a$ versus $|\Delta|^2$ (arbitrary units) for the case with multiple solutions (dashed lines). The minimum energy solution is shown as the thick black line. The areas labelled by A and B are equal.

We thus get

$$\frac{m}{4\pi\hbar^2} d\left(\frac{1}{a}\right) = d\left(\frac{1}{g}\right), \tag{A.3}$$

and therefore

$$\left.\frac{\partial E}{\partial(1/a)}\right|_{N_\sigma} = -V\frac{m}{4\pi\hbar^2}|\Delta(a)|^2. \tag{A.4}$$

Writing this derivative to be $\mathcal{E}'$, we then get the thermodynamic relation

$$\mathrm{d}E = \sum_\sigma \mu_\sigma \mathrm{d}N_\sigma + \mathcal{E}'\mathrm{d}\left(\frac{1}{a}\right). \tag{A.5}$$

The free energy $\Omega(\mu_\sigma, a) \equiv E - \mu_\uparrow N_\uparrow - \mu_\downarrow N_\downarrow$ then obeys

$$\mathrm{d}\Omega = -\sum_\sigma N_\sigma \mathrm{d}\mu_\sigma + \mathcal{E}'\mathrm{d}\left(\frac{1}{a}\right). \tag{A.6}$$

We thus conclude that, for volume V and chemical potentials μ_σ,

$$\left.\frac{\partial\Omega}{\partial(1/a)}\right|_{\mu_\sigma} = -V\frac{m}{4\pi\hbar^2}|\Delta|^2. \tag{A.7}$$

Though this expression is already sufficient to determine and thus compare the free energies of the different solutions for given scattering length a, we can convert it to an even more convenient form. To do this, let us write $x \equiv |\Delta|^2$ and $y \equiv 1/a$. We get, up to an overall multiplying factor

$$\frac{\partial\Omega}{\partial y} = -x. \tag{A.8}$$

Thus, when the solutions are plotted in the form of figure A.1, the free energy Ω of a state can be related to the free energy Ω_0 of another state along the same curve by, again up to an overall multiplicative constant,

$$\Omega = \Omega_0 - \int x\,\mathrm{d}y. \tag{A.9}$$

Since $\int x\mathrm{d}y$ is the area between the curve and the y-axis, the states corresponding to the minimum free energy at a given scattering length a (hence y) can be found via the same procedure as the usual Maxwell construction.

Appendix B. BEC limit

Here we try to understand the behaviour of the density profile in the BEC ($1/k_F a \gg 1$) limit, for the special case of a small number of excess fermions (e.g. figure 1(g)). For a bulk system, it is straightforward to perform a low density expansion of the mean-field equations and obtain an expansion of the chemical potentials $\mu_f \equiv \mu_\uparrow$ and $\mu_b \equiv \mu_\uparrow + \mu_\downarrow$ as a series in the densities $n_f = n_d$ and $n_b \equiv n_\downarrow$ (see [22] for the details of this calculation). In the BEC limit, n_d can be interpreted as the density of the excess unpaired fermions and n_b as the density of the bosons which represent the bound fermion pairs. μ_f and μ_b can be interpreted as the corresponding chemical potentials. Explicitly we have an expansion of the form

$$\mu_f = A n_d^{2/3} + g_{bf} n_b, \tag{B.1}$$

$$\mu_b = -\epsilon_b + g_{bb} n_b + g_{bf} n_f, \tag{B.2}$$

where we have dropped the terms of higher order in the densities. These terms are smaller in the limit $n_f a^3 \ll 1$ and $n_b a^3 \ll 1$. We obtain [22] $A = (6\pi^2)^{2/3}/2m$, $\epsilon_b = \hbar^2/ma^2$, $g_{bb} = 4\pi\hbar^2 a/m$, $g_{bf} = 8\pi\hbar^2 a/m$. The value of A is as expected for a free Fermi gas and ϵ_b is the binding energy of the fermion pair. The values of g_{bb} and g_{bf} here, obtained from the mean-field equations, differ from the correct values known. Exact three-body calculation [23] gives $g_{bf}^{\text{exact}} = 3.6\pi\hbar^2 a/m$, while a recent four-body calculation [24] gives $g_{bb}^{\text{exact}} = 1.2\pi\hbar^2 a/m$. Alternatively, defining the scattering lengths in the usual manner, our low density expansion yields the effective values $a_{bf} = 8a/3$ and $a_{bb} = 2a$, whereas the exact values should be $a_{bf}^{\text{exact}} = 1.2a$ and $a_{bb}^{\text{exact}} = 0.6a$. The difference between the mean-field and exact results is due of course to the approximate nature of the mean-field theory. We note here, however, that (a) a_{bf} and a_{bb} are both positive and of order a, hence in the BEC limit we have necessarily $n_d a^3 \ll 1$, thus the fermions and the bosons can mix [25]; (b) $g_{bf}/g_{bb} > 1/2$ for both mean-field and exact values. We shall explain the importance of this second relation below.

In the trap, equations (B.1) and (B.2) become

$$\mu_f = A n_d(\vec{r})^{2/3} + g_{bf} n_b(\vec{r}) + V(\vec{r}) \tag{B.3}$$

$$\mu_b = -\epsilon_b + g_{bb} n_b(\vec{r}) + g_{bf} n_f(\vec{r}) + 2V(\vec{r}). \tag{B.4}$$

Here $V(\vec{r})$ is the trap potential. We shall only consider the case where the potential increases from the centre of the trap. To appreciate the implications of relation (b), consider the limit of a small number of fermions. The density profile of the bosons can then be determined by first ignoring the fermion term in equation (B.3), and we obtain the boson density profile

$$n_b(\vec{r}) = (\mu_b + \epsilon_b - 2V(\vec{r}))/g_{bb}, \tag{B.5}$$

if the RHS is larger than zero, and $n_b = 0$ otherwise. For ease of reference, we shall call these two regions 'inside' and 'outside' below.

Equation (B.3) can be rewritten in the form

$$\mu_f = A n_d(\vec{r})^{2/3} + V_{\text{eff}}(\vec{r}), \tag{B.6}$$

where $V_{\text{eff}}(\vec{r}) = V(\vec{r}) + g_{bf} n_b(\vec{r})$ is the effective potential for the fermions. We obtain for the inside region $V_{\text{eff}}(\vec{r}) = V(\vec{r}) + (g_{bf}/g_{bb})(\mu_b + \epsilon_b - 2V(\vec{r}))$, whereas for the outside $V_{\text{eff}}(\vec{r}) = V(\vec{r})$. In the inside region, the position dependence is therefore $-(2g_{bf}/g_{bb} - 1)V(\vec{r})$. From this, it is clear that if $g_{bf} > g_{bb}/2$, then the effective potential is actually larger near $\vec{r} = 0$ than near the edge of the boson cloud. It decreases from the centre of the trap till it reaches the edge of the boson cloud, then it increases again due to the spatial dependence of $V(\vec{r})$. Therefore, we conclude that for $g_{bf}/g_{bb} > 1/2$ the excess fermions lie near the edge of the boson cloud, at least for a small number of fermions [18, 26]. The excess fermions lie near the edge of the cloud (figure 1(g)). Thus a peak in $n_d(\vec{r})$ does *not* indicate phase separation.

Appendix C. Axial density

We here discuss some useful expressions governing the axial density within the local density approximation. Our results here are, to some extent, a further development of those obtained in [14].

In the local density approximation, any quantity, say the density difference $n_{\mathrm{d}}(\vec{r})$, is a function entirely of the local chemical potential $\mu(\vec{r})$ (note that h is a constant). Hence, we can write

$$n_{\mathrm{d}}(\vec{r}) = g(\mu(\vec{r})) \equiv g(\mu(\vec{r}), h) \tag{C.1}$$

for some function g. We here note that any density must be identically zero for sufficiently large and negative chemical potential, and thus $g(\zeta)$ vanishes exactly for sufficiently large and negative argument ζ. It will be convenient to define another function $G(\zeta)$ via

$$G(\zeta) \equiv \int_{-\infty}^{\zeta} \mathrm{d}\zeta' g(\zeta'). \tag{C.2}$$

Consider now for example the radially integrated density (referred afterwards as axial density) difference:

$$n_a(z) \equiv \int \mathrm{d}x\mathrm{d}y n_{\mathrm{d}}(\vec{r}). \tag{C.3}$$

The integral can be written as, for a trap that is cylindrically symmetric with respect to z, $\pi \int_0^\infty \mathrm{d}\rho^2 g(\mu_0 - \frac{1}{2}\alpha_z z^2 - \frac{1}{2}\alpha_\parallel \rho^2)$ where $\rho^2 \equiv x^2 + y^2$. This integral can be expressed in terms of G and thus

$$n_a(z) = \frac{2\pi}{\alpha_\parallel} G\left(\mu_0 - \frac{1}{2}\alpha_z z^2\right). \tag{C.4}$$

This relation can be used to obtain directly the axial density in terms of the function g, without first calculating the density profile in trap and then performing the integration. Moreover, it can also be used to deduce the (unintegrated) density profile once the axial density is given, for example from experiment. To see this, we differentiate equation (C.4) with respect to z, and notice that $G'(\zeta) = g(\zeta)$ evaluated at $\zeta = \mu_0 - \frac{1}{2}\alpha_z z^2$ is directly related to the corresponding density at the coordinate $(0, 0, z)$. Thus we have

$$n_{\mathrm{d}}(0, 0, z) = -\frac{\alpha_\parallel}{2\pi\alpha_z}\frac{1}{z}\frac{\partial n_a(z)}{\partial z}. \tag{C.5}$$

Therefore the actual density for a point on the z axis can be obtained from the axial density. Under the local density approximation, the density at any given point in the trap is a function of the local chemical potential only. Hence we can obtain the actual density at any given point in space provided the axial density is given.

The relation equation (C.5) also shows that, since n_{d} is non-negative, the axial density profile is strictly decreasing (increasing) with z for $z > (<)0$, a result pointed out in [14]. In a region where the density vanishes, then the axial density should be a constant, a result recognized in [14] and [15].

References

[1] Fulde P and Ferrell R A 1964 *Phys. Rev.* **135** A550
Larkin A I and Ovchinnikov Y N 1964 *Zh. Eksp. Teor. Fiz.* **47** 1136
Larkin A I and Ovchinnikov Y N 1965 *Sov. Phys.—JETP* **20** 762 (Engl. Transl.)
[2] Tiesinga E, Verhaar B J and Stoof H T C 1993 *Phys. Rev.* A **47** 4114
Inouye S, Andrews M R, Stenger J, Miesner H-J, Stamper-Kurn D M and Ketterle W 1998 *Nature* **392** 151

Courteille P, Freeland R S, Heinzen D J, van Abeelen F A and Verhaar B J 1998 *Phys. Rev. Lett.* **81** 69
Roberts J L, Claussen N R, Burke J P Jr, Greene C H, Cornell E A and Wieman C E 1998 *Phys. Rev. Lett.* **81** 5109
[3] Carlson J and Reddy S 2005 *Phys. Rev. Lett.* **95** 060401
[4] Pao C-H, Wu S-T and Yip S-K 2006 *Phys. Rev.* B **73** 132506
[5] Sheehy D E and Radzihovsky L 2006 *Phys. Rev. Lett.* **96** 060401
Son D T and Stephanov M A 2005 *Preprint* cond-mat/0507586
[6] Eagles D M 1969 *Phys. Rev.* **186** 456
Leggett A L 1980 *Modern Trends in the Theory of Condensed Matter* ed A Pekalski and J Przystawa (Berlin: Springer)
[7] Sá de Melo C A R, Randeria M and Engelbrecht J R 1993 *Phys. Rev. Lett.* **71** 3202
[8] Forbes M M, Gubankova E, Liu W V and Wilczek F 2005 *Phys. Rev. Lett.* **94** 017001 and references therein
[9] Bedaque P F, Caldas H and Rupak G 2003 *Phys. Rev. Lett.* **91** 247002
[10] Caldas H 2004 *Phys. Rev.* A **69** 063602
[11] Zwierlein M W, Schirotzek A, Schunck C H and Ketterle W 2006 *Science* **311** 492
[12] Partridge G B, Li W, Kamar R I, Liao Y and Hulet R G 2006 *Science* **311** 503
[13] Yi W and Duan L-M 2006 *Phys. Rev.* A **73** 031604 (*Preprint* cond-mat/0601006)
[14] De Silva T N and Mueller E J 2006 *Phys. Rev.* A at press (*Preprint* cond-mat/0601314)
[15] Haque M and Stoof H T C 2006 *Preprint* cond-mat/0601321
[16] Chevy F 2006 *Phys. Rev. Lett.* **96** 130401 (*Preprint* cond-mat/0601122)
[17] Kinnunen J, Jensen L M and Törmä P 2006 *Phys. Rev. Lett.* **96** 110403 (*Preprint* cond-mat/0512556)
[18] Pieri P and Strinati G C 2006 *Phys. Rev. Lett.* **96** 150404 (*Preprint* cond-mat/0512354)
[19] Bruun G, Castin Y, Dum R and Burnett K 1999 *Eur. J. Phys.* D **7** 433
[20] Wu S-T and Yip S-K 2003 *Phys. Rev.* A **67** 053603
[21] Abrikosov A A, Gorkov L P and Dzyaloshinskii I E 1965 *Quantum Field Theoretical Methods in Statistical Physics* (Oxford: Pergamon)
Lifshitz E M and Pitaevskii L P 1980 *Statistical Physics* Part 2 (Pergamon: Oxford) Chapter 5, sec 40 (Note however that our sign convention for g is opposite to these references)
[22] Yip S K 2002 *Preprint* cond-mat/0203582
[23] Skorniakov G V and Ter-Martirosian K A 1956 *Zh. Eksp. Teor. Fiz.* **31** 775
Skorniakov G V and Ter-Martirosian K A 1957 *Sov. Phys.—JETP* **4** 648 (Engl. Transl.)
[24] Petrov D, Salomon C and Shlyapnikov G V 2004 *Phys. Rev. Lett.* **91** 090404
[25] Viverit L, Pethick C J and Smith H 2000 *Phys. Rev.* A **41** 053605
[26] Carr L D, Chiaramonte R and Holland M J 2004 *Phys. Rev.* A **70** 043609